

2006

## Silicon Microdosimetry in Heterogeneous Materials: Simulation and Experiment

A. Wroe

*University of Wollongong*

Anatoly B. Rosenfeld

*University of Wollongong, anatoly@uow.edu.au*

I. Cornelius

*University of Wollongong, iwan@uow.edu.au*

Dale A. Prokopovich

*ANSTO, Australia, dap11@uow.edu.au*

M. Reinhard

*ANSTO, Australia*

*See next page for additional authors*

Follow this and additional works at: <https://ro.uow.edu.au/engpapers>



Part of the [Engineering Commons](#)

<https://ro.uow.edu.au/engpapers/330>

---

### Recommended Citation

Wroe, A.; Rosenfeld, Anatoly B.; Cornelius, I.; Prokopovich, Dale A.; Reinhard, M.; Schulte, R.; and Bashkirov, V.: Silicon Microdosimetry in Heterogeneous Materials: Simulation and Experiment 2006.  
<https://ro.uow.edu.au/engpapers/330>

---

**Authors**

A. Wroe, Anatoly B. Rosenfeld, I. Cornelius, Dale A. Prokopovich, M. Reinhard, R. Schulte, and V. Bashkirov

# Silicon Microdosimetry in Heterogeneous Materials: Simulation and Experiment

A. Wroe, *Student Member, IEEE*, A. Rosenfeld, *Senior Member, IEEE*, I. Cornelius, *Member, IEEE*, D. Prokopovich, *Student Member, IEEE*, M. Reinhard, *Member, IEEE*, R. Schulte, and V. Bashkirov

**Abstract**—Microdosimetry spectra obtained experimentally utilizing a Silicon-On-Insulator (SOI) microdosimeter within biological materials, was used to provide information on secondary radiation spectra at tissue boundaries. Comparative GEANT4 simulations of the experimental conditions were also conducted.

**Index Terms**—GEANT4, microdosimetry, protons.

## I. INTRODUCTION

THE determination of biological doses for astronauts and single event upset (SEU) in micro and nano electronics are going to be important goals for world space organizations in the 21st century. One method that can be employed in these studies is microdosimetry, especially the use of solid state microdosimeters such as those that have been developed at the Centre for Medical Radiation Physics (CMRP) at the University of Wollongong. This approach to microdosimetry utilizes Silicon-On-Insulator technology (SOI) and comprises of a 2D-diode array of well-defined sensitive volumes.

The main advantage of silicon microdosimeters for space and aircraft operation is their compact size and low voltage for operation. However, previously they have suffered the drawback of the lack of a well-defined sensitive volume (SV). This new approach utilizing Silicon-On-Insulator (SOI) technology results in microscopically small sensitive volumes (SV's). The structure of this device is illustrated in Fig. 1. The device consists of four arrays, each of differing cell number, and cell cross sectional area so that a suitable array for most conditions is available. A SOI microdosimeter, comprising four separate arrays of up to  $10^4$  silicon cells with a physical size of  $30 \times 30$  or  $100 \times 100$  microns on a single chip with a SV thickness of 2, 5, and 10 microns has been built and has been tested under a number of different incident radiations [1]–[3].

Scaling of the mean chord length allows derivation of tissue-equivalent microdosimetric spectra. Equivalent dose or relative biological effectiveness (RBE) of a radiation field can

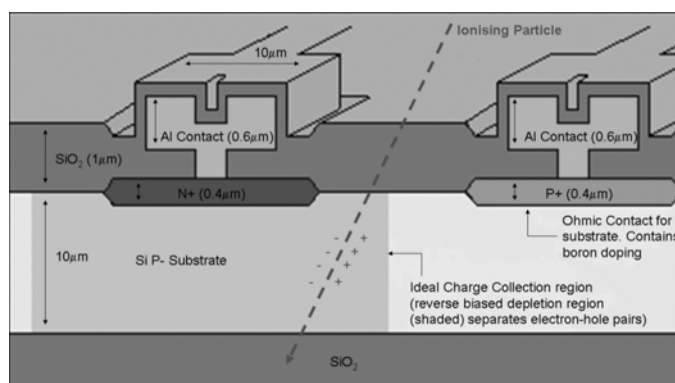


Fig. 1. Basic SOI diode array structure of the microdosimeter used at the CMRP, University of Wollongong.

then be determined by convolution of microdosimetric spectra with quality coefficients within the range of lineal energies in a particular radiation field [4]. The microscopically small cell size is also useful in determining single event upsets (SEU's) in microelectronics, allowing sufficient shielding to be constructed thus enabling long deployments of these devices.

Previously SOI microdosimeters have undergone Monte Carlo simulation studies within homogeneous phantoms and the results compared with experimental data obtained in neutron and proton radiation fields [1]–[3]. These studies have illustrated that such simulations yield useful and accurate information. However, in these cases experimental information has only been obtained for homogeneous Perspex and water phantoms. It is desirable to obtain information utilizing more complex layered heterogeneous structures of biologically important materials for a number of disciplines such as radiation protection including space exploration. Such studies can better develop our understanding of radiation interactions within the body and the changes to the radiation spectra as it traverses a sample of biological material such as a human. This in turn can then be utilized to better construct radiation shielding in radiation protection applications such as those encountered in space.

The aim of this work is to observe the changes in microdosimetry spectra as proton radiation traverses biologically important structures such as the human head and chest. These results will be compared with simulation studies utilizing the GEANT4.7.1 Monte Carlo toolkit [5] for validation. The experimental validation of the GEANT4 Monte Carlo toolkit for heterogeneous commercial phantoms will allow for future simulation studies utilizing actual ICRU tissue equivalent structures.

Manuscript received July 14, 2006; revised September 19, 2006. This work was supported in part by the Australian Institute for Nuclear Science and Engineering (AINSE) and the Australian/American Fulbright Association.

A. Wroe, A. Rosenfeld, and I. Cornelius are with the Centre for Medical Radiation Physics, University of Wollongong, Wollongong, NSW 2087, Australia (e-mail: ajw16@uow.edu.au; anatoly@uow.edu.au; iwan@uow.edu.au).

D. Prokopovich and M. Reinhard are with the Australian Nuclear Science and Technology Organization, Menai, NSW 2234, Australia (e-mail: dpr@ansto.gov.au; mrz@ansto.gov.au).

R. Schulte and V. Bashkirov are with Loma Linda University Medical Center, Loma Linda, CA 92354 USA (e-mail: rschulte@dominion.llumc.edu; vbashkirov@dominion.llumc.edu).

Digital Object Identifier 10.1109/TNS.2006.885797

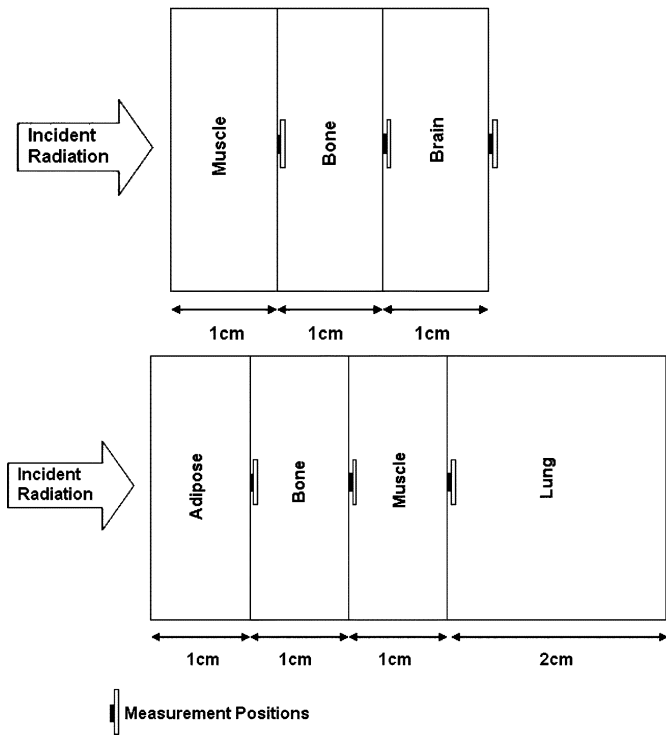


Fig. 2. Schematic diagram of the phantom configuration as used within the experimental and theoretical portion of this work. Note the microdosimeter positions indicating the position of measurement (or simulated measurement) in each case. In the case of 250 MeV proton irradiations, 25 and 50 mm thicknesses of Perspex were also interspaced between the bone and brain layer (in the case of the head phantom) to provide additional measurement points at greater depths in brain.

## II. EXPERIMENTAL METHOD

For this study a tissue equivalent (TE) phantom was specially constructed. It consisted of  $20 \times 20 \times 1 \text{ cm}^3$  slices of adipose, lung, brain, bone and muscle that were layered in a given order such that it could be configured to represent the structure of the human head and chest. The structure of these phantoms is outlined below and in Fig. 2. The compositions of these phantoms were provided by the manufacturer.

- **Head:** 10 mm muscle, 10 mm bone, 10 mm brain (in the case of 250 MeV protons 25–50 mm Perspex [6] is also added to simulate a greater depth in brain).
- **Chest:** 10 mm adipose, 10 mm bone, 10 mm muscle, 20 mm lung.

A  $10 \mu\text{m}$  thick SOI microdosimeter would be used in this study. The array chosen in this experiment comprises of 4800 detector elements ( $40 \times 120$ ) with each cell having a physical size of  $30 \mu\text{m} \times 30 \mu\text{m}$  and a junction size of  $10 \mu\text{m} \times 10 \mu\text{m}$ . The device was contained within a 0.9 mm thick probe holder of aluminum which would act as a Faraday cage. A  $4 \mu\text{m}$  aluminum window was located immediately in front of the microdosimeter to allow the transport of secondary particles into the SV. To enable reproducible placement of the microdosimeter probe in the centre of the radiation field at tissue boundaries, it was housed within a purpose built Perspex probe holder. The probe was then placed at the tissue boundaries within this phantom to ascertain the changes in microdosimetry spectra as a result of changing

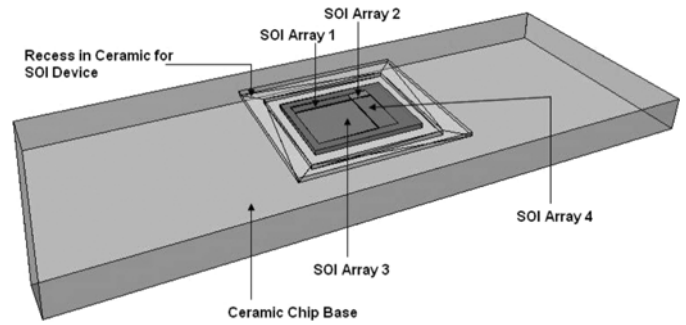


Fig. 3. Schematic of the SOI microdosimeter chip as recreated within the GEANT4 based application. Note the four separate SOI microdosimetry arrays.

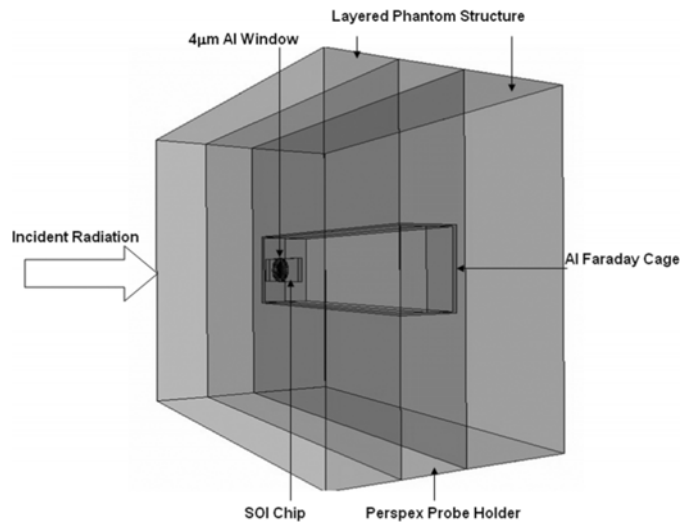


Fig. 4. Schematic of the experimental setup as recreated within the GEANT4 based application.

biological material when irradiated with 100 and 250 MeV protons on the central NASA research beam-line at Loma Linda University Medical Center (LLUMC).

Experimental measurements were conducted with beam sizes of the order of 50 mm diameter at the point of entry into the phantom for 10 minutes. During this time the dead time was kept stable at 10% with a low noise threshold set on the Multi-Channel Analyzer (MCA) of 9 keV. Throughout the course of the experiment the device was irradiated with 0.2–0.35 cGy per spill (accelerator delivered radiation pulse of approximately 0.3 s duration with a total cycle time of 2 seconds in duration). The dose was monitored at regular intervals with a calibrated ion chamber, which has  $12 \mu\text{m}$  entrance and exit windows, a 1.58 mm SV thickness, and is described in [7].

## III. MONTE CARLO SIMULATION

The experimental setup was recreated within an application that was based on the GEANT4.7.1 Monte Carlo Toolkit. This included not only the SOI microdosimeter chip (as represented in Fig. 3), but also the aluminum faraday cage, Perspex probe holder and layered phantom structure. The experimental set-up which was constructed within the GEANT4 based application is seen in Fig. 4.

The commercially available phantoms were reproduced within the simulation program according to the manufacturer's specifications for accurate comparison with simulated results. Energy depositions within the  $10\mu\text{m}$  SOI device were scored to create a MCA spectrum for comparison with the experimental results. This comparison was used to determine the accuracy of the GEANT4 based application in simulating the response of the microdosimeter within commercially available TE phantoms.

The Physics processes utilized for the transport of light ions (including protons) included low energy inelastic scattering (pre-compound model), low energy ionization (ICRU 49) and multiple scattering models. The physics of secondary particles including photons, electrons, neutrons and nuclear secondaries was also considered and accounted for using the appropriate models. Each simulation was carried out for  $2 \times 10^7$  normally incident protons transported along an evacuated beam pipe, beam exit window and across a 3.5 m air gap into the phantom and experimental probe assembly. In the case of the 250 MeV simulations, a thin lead scattering foil was used to achieve a larger, more uniform field at the phantom. This was also included in calculations.

#### IV. RESULT NORMALIZATION

In comparing the simulated and experimental results for validation it is important that adequate normalization occurs. The experimental results were binned into 2048 channels by the MCA. An energy calibration was applied to the experimental results, that was derived using a calibrated pulser, which in turn was calibrated using a  $350\mu\text{m}$  thick planar Silicon detector of similar capacitance to the microdosimetry detector array to be used and an Am-241 source.

The simulated results were binned into 8000 bins spanning an energy range of 0–4 MeV. The simulated results then had a charge collection efficiency (CCE) of 0.8 applied which has been previously determined and verified through ion beam induced charge collection studies (IBICC)[8]. The simulated results were then convolved with a Gaussian of  $\sigma = 5\text{ keV}$  (measured experimentally) to reflect the electronic noise present in the system (see equation below).

$$f_j = \sum_{i=j-3\sigma}^{j+3\sigma} \frac{1}{\sqrt{2\sigma^2\pi}} f_i \exp - \frac{(\varepsilon_j - \varepsilon_i)^2}{2\sigma^2}.$$

Where  $\varepsilon_i$  is the energy values corresponding to bin  $i$  of the frequency distribution.

Finally, both the simulated and experimental results were normalized to the total number of events present above twice the noise threshold of the experimental device. In this case the noise threshold of the experimental device was measured to be 15 keV, as such the results were normalized to total number of events higher than 30 keV.

#### V. MICRODOSIMETRY SPECTRA GENERATION

Once validation of the GEANT4 based application had occurred the raw simulated data would be converted into microdosimetry spectra using the protocol outlined in [4]. A mean

chord length of  $\langle l \rangle = 19.05\mu\text{m}$  was used for these calculations. This value was based on a  $30 \times 30 \times 10\mu\text{m}^3$  volume and a tissue equivalent scaling factor of  $\zeta = 0.63$ ;

$$\langle l \rangle = \frac{4V}{S\zeta}.$$

Where  $V$  is the volume,  $S$  is the total surface area,  $\zeta$  is the equivalent scaling factor,  $\langle l \rangle$  the mean chord length.

The spectra produced gives the fraction of the total dose occurring from lineal energy events in the interval  $y \rightarrow y+dy$  where  $y$  is the lineal energy in  $\text{keV}/\mu\text{m}$ . Viewing the mean dose weighted lineal energy at each tissue boundary would give an indication of changes to microdosimetry spectra as a function of preceding material.

#### VI. VALIDATION RESULTS AND DISCUSSION

The experimental measurements were completed on the central NASA research beam-line at LLUMC. Experimental results for all energy/phantom combinations are unobtainable below 15 keV due to the noise limit of the device. This lower level noise limit is clearly evident in all the graphs displayed.

Fig. 5 shows a comparison between simulated and experimental results. A discontinuity is observed in the simulated case at approximately 140 keV. The simulated case has a sharp drop before continuing parallel to the experimental trend at higher energy values. This is observed for all 100 MeV simulations, yet no discontinuity is observed for 250 MeV incident proton energy. Possible explanations for the discontinuity are:

- A discontinuity in the physics models for lower proton energies regarding nuclear reactions. However, as the same models are used for the higher energy simulations with no discontinuity observed this seems unlikely.
- The range cut in electron transport preventing low energy electrons for depositing energy in the device. However, as the same cut is used for the higher energy simulations with no discontinuity observed this seems unlikely.
- An overestimation in the device overlayer in the simulated case. The simulated overlayer was constructed within the GEANT4 simulation to be a uniform layer of  $\text{SiO}_2$  with a  $1\mu\text{m}$  thickness. In actual fact it may have regions of varying thickness and possibly composition. Also the aluminum contacts were not contained within the simulation which could lead to errors in particle transport into the SV. Such errors could cause low energy protons to be prevented in reaching the SV. This would be seen causing a greater impact on 100 MeV results as nuclear secondaries (including recoil protons) produced would have a lower energy, which would be affected to a greater degree by inaccurate overlayer simulation.

Figs. 6 and 7 show the comparison between experimental and simulated spectra for 250 MeV protons incident on the head phantom and chest phantom, respectively. The agreement between the simulated and experimental cases is best in the region of 15–80 keV with almost no discrepancy. In the region of 80–500 keV there is some discrepancy between the simulated and experimental data, which can be as large as a factor of 2–3. This difference is most likely due to an oversimplification in the

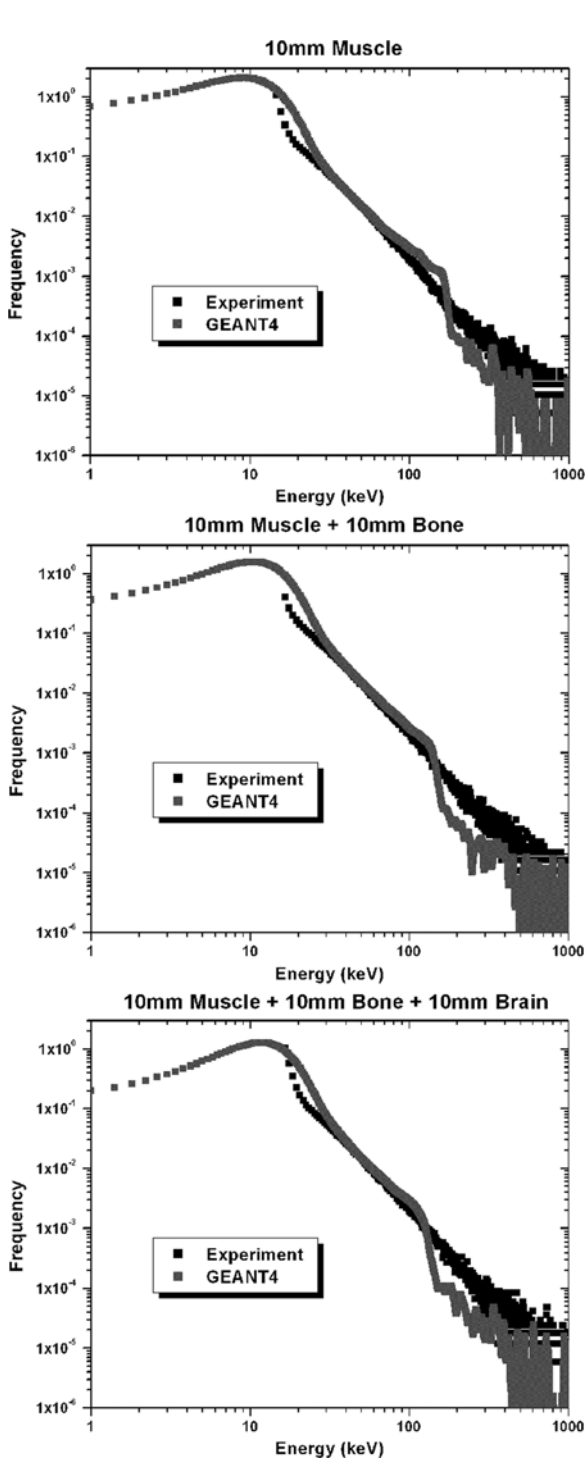


Fig. 5. Comparative experimental and simulation results for the head phantom, when irradiated with 100 MeV protons.

simulation in the device overlayer as in the case of high linear energy transfer (LET)/low range secondaries an incorrectly simulated overlayer could result in error in their transport and hence energy deposition within the SV.

It is also important to note that this difference is most pronounced for the first 10 mm layer of each phantom structure. This amplification in the discrepancy is most likely caused by an overestimation of the beam divergence as it travels along the

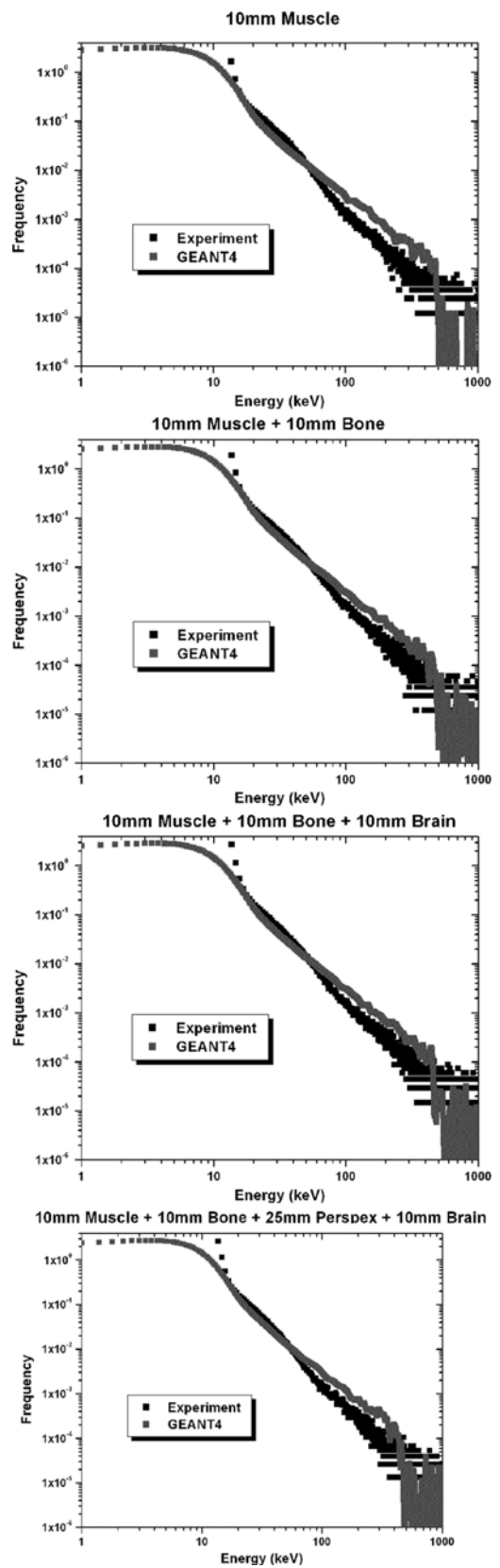


Fig. 6. Comparative experimental and simulation results for the head phantom, when irradiated with 250 MeV protons.

beam pipe towards the experimental set-up. Such high discrepancies are only observed in the first 10 mm of the phantom, as

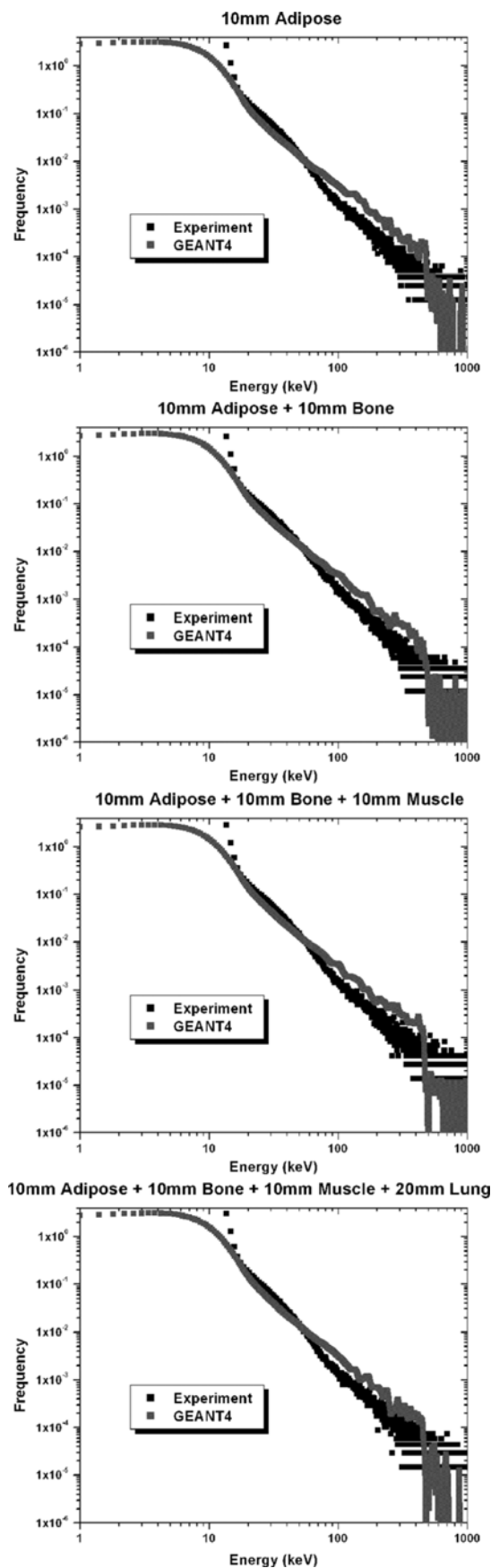


Fig. 7. Comparative experimental and simulation results for the chest phantom, when irradiated with 250 MeV protons.

small initial beam divergence errors are nullified at depth within the phantom due to internal scatter of the incident protons. Despite this discrepancy the trend of the experimental results are well represented by the simulation for all phantom material configurations.

In the case of the head phantom for 250 MeV incident protons a 25 mm thick Perspex slab was used to simulate a greater depth within the brain. However, in this case the brain slab was re-orientated to remain the last layer of the phantom immediately before the microdosimeter probe assembly. This would ensure that any short range secondaries produced by the brain phantom would be transported and detected by the device, not attenuated by Perspex.

## VII. MICRODOSIMETRY RESULTS AND DISCUSSION

Although some discrepancy was observed between the simulated and experimental cases for higher energy deposition events, the experimental trend/response of the microdosimeter (a complex radiation device) was well reflected in the simulation. The advantage which the simulation provides over the experimental device is that we can simulate a device with no electronic noise and no lower level noise threshold.

The simulated results with no noise convolution or charge collection applied were converted into dose weighted lineal energy spectra according to the protocol outlined in [4]. For each conversion the results were normalized to the total number of energy deposition events. Due to the small changes in microdosimetry spectra as a function of phantom material upstream of the microdosimeter, a good parameter to observe any change is the mean dose weighted lineal energy. These are presented in Tables I and II for the case of 250 MeV protons irradiating the head and chest phantom. The advantage of using 250 MeV protons for this study is that all simulated measurement positions took place within the plateau region, before the Bragg Peak. As such the changes in lineal energy are mostly caused by the changing phantom material rather than the slowing of the proton in the Bragg peak region.

In the case of the head phantom it is clear that there is a variation in the mean dose weighted lineal energy as a result of the preceding TE slab. Measurements immediately behind the bone (see Fig. 2) boundary result in an increase in mean dose weighted lineal energy of approximately 23%. An elevated value is also recorded at 10 mm depth within brain before returning to more stable values at greater depths within the TE brain phantom as simulated by additional layers of Perspex.

This increase in lineal energy as a result of the bone boundary is a possible indication of increased RBE in this region. The higher lineal energies simulated are a direct consequence of an increased level of inelastic scatter producing scattered low energy protons and high LET inelastic secondaries within the bone layer. This elevated lineal energy value is also experienced at 10 mm depth in brain before returning to more stable values. This increase in lineal energy as a result of the bone layer could result in increased radiation damage in cells and tissues

In the simulation of the mean dose weighted lineal energy within the chest phantom, the same trend is seen as in the head phantom. Immediately after the bone layer there is an increase in lineal energy which continues to greater depth within the

TABLE I  
MEAN DOSE WEIGHTED LINEAL ENERGY VALUES FOR SIMULATED  
MEASUREMENT POSITIONS WITHIN THE HEAD PHANTOM WHEN IRRADIATED  
WITH 250 MEV PROTONS

Position	$\bar{y}_d$ (keV / $\mu\text{m}$ )
Muscle/Bone Interface	4.75171
Bone/Brain Interface	5.84671
10mm Depth Brain	5.65041
35mm Depth Brain	4.45557
60mm Depth Brain	4.78842

TABLE II  
MEAN DOSE WEIGHTED LINEAL ENERGY VALUES FOR SIMULATED  
MEASUREMENT POSITIONS WITHIN THE CHEST PHANTOM WHEN IRRADIATED  
WITH 250 MEV PROTONS

Position	$\bar{y}_d$ (keV / $\mu\text{m}$ )
Adipose/Bone Interface	5.08208
Bone/Muscle Interface	5.70244
Muscle/Lung Interface	5.79357
20mm Depth Lung	5.38776

phantom (predominantly due to the low density of the TE lung phantom).

Another interesting trend observed in these results occurs in both phantoms after only 10 mm of material. In the case of the head phantom muscle is the most anterior (i.e., closest to the incident radiation) phantom layer, while in the case of the chest phantom this is adipose. The differing composition of these two layers results in a clear variation in lineal energy. As the main variation of composition in these commercially available TE phantoms is that adipose contains approximately 5% more carbon, it could be concluded that these increased levels of carbon produced increased levels of inelastic scatter resulting in an increased dose weighted mean lineal energy.

We can see clearly from these simulated measurements of dose weighted lineal energy within commercially available TE phantoms that the quality of the proton radiation varies in different tissue substances. To better understand the effect produced by actual tissue materials, simulation studies should be completed utilizing such compositions and lineal energy as the measurement parameter.

## VIII. CONCLUSIONS

The GEANT4.7.1 Monte Carlo Toolkit was used to simulate the MCA spectra obtained with silicon microdosimeter in different locations of commercially available tissue equivalent heterogeneous phantoms irradiated with 100 MeV and 250 MeV protons.

In the case of the 100 MeV head phantom a discrepancy was observed between the experimental and simulated case at approximately 140 keV. This discrepancy took the form of a sharp decrease in response in the simulated spectra, followed by a trend that reflects that of the experimental results.

This is observed for all 100 MeV simulations and could be caused by with a discontinuity in the physics models of the sim-

ulation in this energy range and incorrect simulation of the device overlayer.

Both the chest and head phantoms were irradiated with 250 MeV protons and no discontinuity in the simulated spectra was observed in this case. Minimal variation between the two spectra was observed below 80 keV energy depositions, while at higher energy depositions within the device a discrepancy of factor 2–3 was observed. A detailed simulation of the devices overlayer could result in a higher level of accuracy in this region, especially in the case of high LET/low range secondaries.

The next step in this work was to use the raw simulation results (with no noise convolution to reflect the experimental case) to ascertain changes in lineal energy as a function of upstream material. Such analysis showed clear variation in mean dose weighted lineal energy as a function of tissue boundary. In both the case of the chest and the head phantom, when irradiated with 250 MeV protons there was a clear increase (as high as 23%) in the mean lineal energy immediately after the bone layer. In both cases this increase in lineal energy continued into the following tissue layers and would suggest an increase in cell death or mutation in this region. This increase in lineal energy is most likely the caused by increased levels of inelastic scatter producing scattered low energy protons and high LET inelastic secondaries within the bone layer.

Another interesting trend seen in the simulated lineal energy spectra was an increase in lineal energy when comparing muscle to adipose at the same depth for the same irradiation condition. Such an increase can be attributed to the composition difference of the two producing a different spectrum of secondary particles. This illustrates the importance of material composition on the secondary radiation spectra and how microdosimetry provides an assessment of radiation quality at different points within a radiation field.

This work has highlighted the benefit of utilizing experimental measurements to verify GEANT4 based simulations of heterogeneous targets. The simulation program can then be used to provide an estimate of lineal energy and to assess the secondary particle spectra produced by such structures. Such measurements and simulations may allow for optimization of shielding structures for radiation protection applications such as space travel and exploration, and may provide a much more effective assessment of shielding performance than absorbed dose alone.

## IX. FURTHER WORK

This work has demonstrated the applicability of GEANT4 based simulations to study the response of the SOI microdosimeter. It is clear from this research that changes in lineal energy occur at different tissue boundaries that depend on the preceding material. Further work should be conducted in extending these results to actual ICRU tissue equivalent compositions.

## ACKNOWLEDGMENT

The authors would like to thank the Australian Nuclear Science and Technology Organization (ANSTO), especially the as-

sistance of Associate Prof. D. Alexiev. The accelerator staff at LLUMC provided invaluable support and expertise for this project. Acknowledgement must also be extended to the National Space Biomedical Research Institute (NSBRI) and our collaborators J. Dicello and V. Pisacane for their support and useful discussion on this research.

#### REFERENCES

- [1] A. B. Rosenfeld, P. D. Bradley, I. Cornelius, B. J. Allen, M. Zaider, R. L. Maughan, J. C. Yanch, J. Coderre, J. B. Flanz, and T. Kobayashi, "Solid state microdosimetry in hadron therapy," *Radiat. Protection Dosimetry*, vol. 101, pp. 431–434, 2002.
- [2] P. D. Bradley, A. B. Rosenfeld, and M. Zaider, "Solid state microdosimetry," *Nucl. Instrum. Methods Phys. Res. B*, vol. B184, pp. 135–157, 2001.
- [3] A. B. Rosenfeld, P. D. Bradley, I. Cornelius, G. I. Kaplan, B. J. Allen, J. B. Flanz, M. Goitein, A. Van Meerbeeck, J. Schubert, J. Bailey, Y. Takada, A. Maruhashi, and Y. Hayakawa, "A new silicon detector for microdosimetry applications in proton therapy," *IEEE Trans. Nucl. Sci.*, vol. 47, pp. 1386–1394, Aug. 2000.
- [4] "Microdosimetry," in *Int. Commission on Radiation Units and Measurements*. Bethesda, MD: ICRU, 1983, vol. 36, ..
- [5] S. Agostinelli, J. Allison, and K. Amako, "GEANT4—A simulation toolkit," *Nucl. Instrum. Methods Phys. Res. A*, vol. A506, pp. 250–303, 2003.
- [6] National Institute of Standards and Technology PSTAR Database Program [Online]. Available: <http://physics.nist.gov/cgi-bin/Star/compos.pl?ap>
- [7] V. Bashkirov and R. W. Schulte, "Dosimetry system for the irradiation of thin biological samples with therapeutic proton beams," *Phys. Med. Biol.*, vol. 47, pp. 409–420, 2002.
- [8] I. Cornelius, R. Siegele, A. B. Rosenfeld, and D. D. Cohen, "Ion beam induced charge characterisation of a silicon microdosimeter using a heavy ion microprobe," *Nucl. Instrum. Methods Phys. Res. B*, vol. B190, pp. 335–338, 2002.